International Journal of Pharmaceutics 618 (2022) 121665

Contents lists available at ScienceDirect

International Journal of Pharmaceutics

journal homepage: www.elsevier.com/locate/ijpharm

Design of red blood cell membrane-cloaked dihydroartemisinin nanoparticles with enhanced antimalarial efficacy

Hengtong Zuo [a,1], Jihong Qiang [a,1], Yidan Wang [a], Rongrong Wang [a], Geng Wang [a], Liqing Chai [a,b], Guolian Ren [a], Yongdan Zhao [a], Guoshun Zhang [a,*], Shuqiu Zhang [a,*]

[a] School of Pharmacy, Shanxi Medical University, Taiyuan 030001, China
[b] Shanxi Provincial People's Hospital, Taiyuan, 030012, China

ARTICLE INFO

Keywords:
Malaria
Dihydroartemisinin
Biomimetic nanoparticles
Long circulation
Targeting

ABSTRACT

Targeting delivery and prolonging action duration of artemisinin drugs are effective strategies for improving antimalarial treatment outcomes. Here, dihydroartemisinin (DHA) loaded poly (lactic-*co*-glycolic acid) (PLGA) nanoparticles (PDNs) were prepared and further cloaked with red blood cell (RBC) membranes via electrostatic interactions to yield RBC membrane-cloaked PDNs (RPDNs). The prepared RPDNs displayed a notable "core-shell" structure, with a negative surface charge of −29.2 ± 4.19 mV, a relatively uniform size distribution (86.4 ± 2.54 nm, polydispersity index of 0.179 ± 0.011), an average encapsulation efficiency (70.1 ± 0.79%), and a 24-h sustained-release behavior *in vitro*. Compared with PDNs, RPDNs showed markedly decreased phagocytic activity by RAW 264.7 cells and had prolonged blood circulation duration. The Pearson correlation coefficient of RPDNs distribution in infected red blood cells (iRBCs) was 0.7173, suggesting that RPDNs could effectively target *Plasmodium*-iRBCs. In *Py*By265-infected mice, RPDNs showed a higher inhibition ratio (88.39 ± 2.69%) than PDNs (83.13 ± 2.12%) or DHA (58.74 ± 3.78%), at the same dose of 8.8 μmol/kg. The ED_{90} of RPDNs (8.13 ± 0.18 μmol/kg) was substantially lower than that of PDNs (14.48 ± 0.23 μmol/kg) and DHA (17.67 ± 3.38 μmol/kg). Furthermore, no apparent abnormalities were detected in routine blood examination, liver function indexes, and pathological analysis of tissue sections of *Py*By265-infected mice following RPDNs treatment. In conclusion, the prepared RPDNs exhibited enhanced antimalarial efficacy, prolonged circulation, targeted delivery to *Plasmodium*-iRBCs, and satisfactory biocompatibility.

1. Introduction

Malaria remains one of the most serious parasitic infectious diseases, with an estimated 229 million clinical cases and 409 000 deaths documented in 2019 (Ashley et al., 2018; Berry-Moorcrof, 2020). Invasion by the malaria parasite causes extensive changes in host red blood cells (RBCs) (Cooke et al., 2004), including alterations in their shape, enhanced membrane permeability, and parasite protein expression in the membrane, thereby facilitating parasite survival within the host RBC (Moxon et al., 2011). In turn, both membrane and cellular changes are responsible for malaria-related symptoms and pathologies, including severe anemia and cerebral malaria (Mohandas and An, 2012).

Artemisinin and its derivatives have been developed as antimalarial drugs and are used worldwide (Efferth, 2017). Dihydroartemisinin (DHA), a first-line antimalarial drug, also as a common active metabolite of most artemisinin-based drugs, exhibits antimalarial activity equivalent to 4–8 times that of artemisinin (Frohlich et al., 2018). However, unsatisfactory physicochemical properties, such as short half-life and low bioavailability, impact its efficacy during antimalarial therapy (Zhang et al., 2018). Accordingly, efficient nano-based drug delivery systems have been designed to overcome these drawbacks (Barabadi et al., 2019; Santos-Magalhaes and Mosqueira, 2010).

Nanotechnology can be used for adjusting the solubility of insoluble drugs, prolonging drug release, and improving drug bioavailability, especially for targeted drug delivery (Aditya et al., 2013; Walvekar et al., 2019). As a miniaturized drug delivery carrier, poly (lactic-*co*-glycolic) acid (PLGA), approved by the US Food and Drug Administration (FDA), has been widely used in nano-drug delivery systems, given its controllable properties, complete biodegradability, and biocompatibility (Ding and Zhu, 2018; Mir et al., 2017). However, conventional

* Corresponding authors.
E-mail addresses: zhangguoshunshun@126.com (G. Zhang), shuqiu.zhang@sxmu.edu.cn (S. Zhang).
[1] These authors contributed equally to this work

https://doi.org/10.1016/j.ijpharm.2022.121665
Received 13 October 2021; Received in revised form 6 March 2022; Accepted 10 March 2022
Available online 12 March 2022

nano-based drug delivery systems assembled with PLGA lack targeting ability and undergo rapid elimination via macrophage uptake (Fang et al., 2018; Zhang et al., 2017).

Recently, cytomembrane-coated nanoparticles with desired features, including high biocompatibility, a prolonged half-life, and disease-specific targeting, have been developed (Luk and Zhang, 2015; Spanjers and Städler, 2020). Various types of cytomembranes, such as RBCs, leukocytes, platelets, stem cells, cancer cells, and hybrid membranes, can be used to prepare biomimetic nanoparticles (Xu et al., 2020). Among these cellular sources of membranes, RBCs are the most abundant in the human body, with approximately 5 million/μL blood (Xia et al., 2019). In addition, *Plasmodium falciparum* erythrocyte membrane protein 1 (*Pf*EMP-1), a parasite-derived antigen expressed on the surface of *Plasmodium*-infected RBCs, can bind to receptors on uninfected RBCs (Dong et al., 2021; Smith et al., 2013; Wahlgren et al., 2017). The adhesion of uninfected RBCs to *Plasmodium*-iRBCs (rosetting) resulted in the parasite invasion to normal RBCs (Ndam et al., 2017; Yam et al., 2017). Thereby, RBC membrane cloaked nanoparticles exhibits relative affinity or targeting to iRBCs (Alanazi et al., 2011; Rowe et al., 2009; Wei et al., 2022). Moreover, the "self-marker" membrane proteins on the RBC membrane bypasses immune surveillance and facilitates prolonged circulation (Hu et al., 2011; Wang et al., 2019; Zhang et al., 2017). Hence, RBC membranes encapsulated nanoparticles is inherently suitable for intravascular drug delivery, such as in antimalarial treatment.

Based on the above-mentioned strategies, an RBC membrane-coated nano-drug delivery system was tentatively designed to optimize the antimalarial effect of DHA. Initially, PLGA nanoparticles were loaded with the antimalarial drug DHA to form a "core" structure (DHA-loaded PLGA nanoparticles; PDNs). Subsequently, RBC vesicles (RVs) were prepared, which was followed by the co-extruded of RVs and PDNs to produce RBC coated "core-shell" structured nanocomplexes (RPDNs). Furthermore, the pharmaceutical properties, antimalarial activity, and biocompatible safety were comprehensively investigated.

2. Materials and methods

2.1. Materials and animals

DHA was purchased from Chongqing Holley Wuling Mountain Pharmaceutical Company (Chongqing, China). PLGA (lactic acid:glycolic acid = 50:50, molecular weight [MW] = 13000 Da) was provided by Jinan Daigang Biomaterial Co. Ltd. (Jinan, China). Vitamin E polyethylene glycol succinate (TPGS) was purchased from Aladdin Biotechnology Co. Ltd. (Shanghai, China). Coumarin-6 (C6) from Beijing Bailingwei Tech. Co. Ltd. (Wuhan, China), Hoechst 33342 from Thermo Fisher Scientific Inc. (Shanghai, China), and 1,19-dioctadecyl-3,3,39,39-tetramethylindodicarbocyanine perchlorate (DiD) and 4′,6-diamidino-2-phenylindole (DAPI) from Boster Biological Technology Co. Ltd. (Shanxi, China). RAW 264.7 cells were procured from the National Center for Nanoscience and Technology (Beijing, China). All other reagents were analytically pure.

For the *in vivo* antimalarial assessment of RBC membrane-cloaked PLGA-DHA nanoparticles (RPDNs), Institute of Cancer Research (ICR) male mice (20–24 g, Laboratory Animal Center of Shanxi Medical University) were used. All animal experiments were conducted in accordance with the Guidelines for the Care and Use of Laboratory Animals of the Shanxi Medical University.

2.2. Preparation of PDNs

PDNs were prepared using a nanoprecipitation method as previously described (Zhu et al., 2014). Briefly, DHA, PLGA, and TPGS, at the determined weights and proportion, were dissolved in dimethylformamide (DMF) solution (0.5 mL). The mixture was added to 2.5 mL of 0.03% (w/v) TPGS solution with gentle stirring for 2 h. The obtained solution was centrifuged at 3500 r/min for 15 min to remove free DHA and PLGA. Next, the nanoparticle dispersion was dialyzed in an aqueous solution with a dialysis bag (MW cut-off [MWCO]: 3500 Da) for 3 h to remove DMF. The PDNs dispersion was maintained at 4 ° C. Instead of DHA, 0.1 wt% DiD or C6 was used for preparing fluorescence-labeled nanoparticles using the earlier described method.

2.3. Optimization of PDNs using response surface methodology (RSM)

A three-factor, three-level Box–Behnken design (BBD) combined with RSM was applied for optimizing the formulation. DHA concentration, mass ratio of TPGS to PLGA, and stirring speed were selected as independent variables. Particle size, zeta potential, and entrapment efficiency (EE) were used as dependent variables. The three experimental factors and three levels of the BBD are shown in Table S1.

2.4. Characterization of PDNs using fourier transform infrared spectroscopy (FT-IR) and differential scanning calorimetry (DSC)

FT-IR spectra of DHA, PLGA, physical mixture (MIX), and PDNs were obtained using a Thermo Nicolet Nexus IS5 FT-IR instrument (Thermo Fisher Scientific, USA). The scan range was set from 1000 to 4000 cm^{-1} at a resolution of 4 cm^{-1} and 16 scans. DSC measurements were performed on a ZCT-B DSC/TGA calorimeter (Jingyi Gaoke Instrument Co. Ltd., Beijing, China) at a dry nitrogen flow rate of 20 mL/min. The temperature ranged from 40 to 250 ° C at a rate of 10 ° C/min.

2.5. Preparation and characterization of RVs

RVs were prepared according to a previously described procedure, with minor modifications (Li et al., 2019). Briefly, whole blood was collected from male ICR mice (6–8 weeks) and centrifuged at 2500 r/min for 5 min at 4 ° C to prepare plasma. The resulting RBCs were washed with ice-cold 1 × phosphate-buffered saline (PBS) three times to remove residual plasma. The washed RBCs were resuspended in 0.25 × PBS for 30 min at 4 ° C to induce RBC expansion and rupture. Subsequently, the obtained RBC solution was centrifuged at 13,000 r/min for 15 min at 4 ° C to remove hemoglobin.

After three wash–centrifugation cycles, the pink pellets were collected. For obtaining RVs, the resulting RBC ghosts were sonicated for 15 min using a sonicator bath (SB-5200DTDN, 42 kHz, 100 W) and further extruded serially through 400-, 200-, and 100-nm polycarbonate porous membranes using an Avanti mini extruder (Genizer). The particle size, polydispersity index (PDI), and zeta potential of the RVs were evaluated using a Malvern Zetasizer Nano ZS unit (Nano ZS90, Malvern, UK). The morphology of the obtained RVs was examined using an inverted microscope and transmission electron microscopy (TEM; JEM-2011F, JEOL, Japan).

2.6. Preparation RPDNs

RVs were coated over the PDNs and subjected to extrusion (Luk et al., 2014). Then, a mixture of PDNs (1 mg) and RVs (from 500 μL whole blood) was ultrasonicated (SB-5200DTDN, 42 kHz, 100 W) for 5 min. To obtain final RPDNs, the mixture suspension was extruded using an Avanti mini extruder (Genizer) through a 200-nm polycarbonate film 15 times.

2.7. Characterization of PDNs and RPDNs

The PDNs and RPDNs dispersions were diluted to 1:10 with double-distilled water. Particle size and zeta potential were determined using a Malvern Zetasizer Nano ZS unit (Nano ZS90, Malvern, UK). PDNs and RPDNs morphologies were characterized using TEM at an accelerating voltage of 200 kV. Briefly, the PDNs and RPDNs dispersions were dropped onto a carbon-coated copper grid, negatively stained with 1% phosphotungstic acid solution, and then air-dried.

2.8. Evaluation of drug-loading capacity, drug release in vitro, and stability

The encapsulation efficiency (EE) and drug-loading capacity (DL) of PDNs were determined using high-speed centrifugation. PDNs dispersions were centrifuged at 13,000 r/min for 15 min. Then, 1 mL of the supernatant was collected, and the PDNs dispersions was ruptured using methanol. High-performance liquid chromatography (HPLC, LC-2030, Shimadzu, Japan) with a post-column derivatization system (LC-10AT, Shimadzu, Japan) was used to measure the DHA concentration (Edlund et al., 1984; Gordi et al., 2000; Melendez et al., 1991). The post-column reaction was conducted with 1 mol/L KOH as the derivatization reagent in a water bath at 70 ° C for approximately 1 min (Ren et al., 2020; Wang et al., 2021). The EE and DL were calculated using the following formula:

$$EE = \frac{Amount\ of\ DHA\ encapsulated\ in\ PDNs}{Total\ amount\ of\ DHA} \times 100\%$$

$$DL = \frac{Amount\ of\ DHA\ encapsulated\ in\ PDNs}{Total\ amount\ of\ PDNs} \times 100\%$$

To evaluate the drug release profile *in vitro*, DHA solution and PDNs and RPDNs dispersions (1 mg/mL, 2 mL) were added to a disposable dialysis bag (MWCO: 3500 Da) placed in PBS (pH = 7.4) with 30% ethanol (20 mL) (Wang et al., 2021). The external drug release buffers were collected, and the same volume of fresh media was added at 0, 0.25, 0.5, 1, 2, 4, 6, 8, 12, and 24 h. The *in vitro* release behavior of PDNs and RPDNs was evaluated using HPLC with post-column derivatization.

The serum stability and preliminary stability of PDNs and RPDNs were examined. Serum stability tests were conducted as previously described (Guo et al., 2015). In brief, the PDNs and RPDNs were added to 100% fetal bovine serum (FBS), and the absorbance values at 560 nm were measured at different time points for detecting particle aggregation in the presence of FBS. PDNs and RPDNs were incubated in water at 4 ° C for 7 days. The samples were collected for dynamic light scattering (DLS) analysis. Particle size and PDI were measured to determine the preliminary stability of PDNs and RPDNs.

2.9. In vitro hemolysis assay

To determine the effect of PDNs and RPDNs on the blood system, a hemocompatibility test was conducted using an *in vitro* hemolysis assay. Human RBCs were centrifuged at 2300 r/min for 15 min. The collected RBCs were washed three times with sterile 0.9% NaCl, and a 2% (v/v) RBC suspension was prepared in 0.9% NaCl. An aliquot of the suspension (2.5 mL) was subsequently incubated with different doses of PDNs and RPDNs in 0.9% NaCl for 3 h at 37 ° C. After incubation, the suspension was centrifuged at 2300 r/min for 15 min. The absorbance of the supernatant was measured using ultraviolet spectrophotometry at 540 nm to examine RBC hemolysis in each group. A sample from the incubated suspension without added PDNs and RPDNs and a sample from the suspension with distilled water (instead of PDNs and RPDNs) served as the negative and the positive control groups, respectively. The hemolysis rate (HR) was calculated as follows:

$$HR = \frac{A(540)_s - A(540)_{nc}}{A(540)_{pc} - A(540)_{nc}} \times 100\%$$

where $A(540)_s$, $A(540)_{nc}$, and $A(540)_{pc}$ are the absorbance values of the samples, negative control groups, and positive control groups at 540 nm, respectively.

2.10. Macrophage uptake assay

Briefly, RAW 264.7 cells were seeded in 96-well plates at a density of 1×10^5 cells per well and cultured in Dulbecco's modified Eagle medium (DMEM) under 5% CO_2 at 37 °C for 24 h. DMEM was removed, and the cells were washed three times with PBS, followed by which PLGA-C6 nanoparticles (PC6Ns) and RBC-PLGA-C6 nanoparticles (RPC6Ns) were added to fresh DMEM at the same mass (100 μg). After incubation for 3 h, the cells were washed with PBS three times, nuclei were stained with DAPI, and the cells were imaged using an ImageXpress Pico Automated Cell imaging system (Molecular Devices Co. Ltd., Shanghai, China). The average granule counts were measured using the Endocytosis Module 2-channel assay for detecting fluorescence (Zhou et al., 2017), and cell uptake was quantitatively analyzed using flow cytometry.

2.11. In vivo blood circulation study

Fluorescently labeled nanoparticles were prepared according to the preparation process used for RPDNs, with DHA replaced by DiD, and then used for simulating the half-life of biomimetic nanoparticles in blood circulation. ICR mice were injected with 200 μL of fluorescently labeled particles through the tail vein. Subsequently, 40 μL of whole blood was collected at 1, 15, and 30 min and 1, 2, 4, 8, 10, 24, 48, and 72 h after injection. Whole-blood samples were diluted with 100 μL of PBS containing active ingredient sodium in 96-well dark plates, and the fluores-cence intensity was determined using a fluorescence microplate reader (Thermo Fisher Scientific, USA).

2.12. In vitro targeting ability of RPDNs

Fluorescently labeled nanoparticles were obtained by loading C6 fluorescence (PC6Ns and RPC6Ns). Blood samples were acquired from ICR mice infected with *Plasmodium yoelii* BY265 (*Py*BY265) at an infection ratio of ≥ 50%, centrifuged at 1500 r/min for 5 min, and washed with PBS three times to obtain iRBCs. PC6Ns and RPC6Ns were added to fresh centrifuge tubes containing iRBCs and RPMI 1640. The fluorochrome Hoechst 33342 was immediately added to the mixture. After incubation for 2 h and rinsing thrice with PBS, the targeting ability of RPC6Ns was evaluated using confocal laser scanning microscopy (Olympus, Japan). Pearson correlation analysis was performed using Scatter J of ImageJ software (National Institutes of Health, Bethesda, MD, USA).

2.13. In vivo antimalarial studies of RPDNs

The antimalarial activities of DHA, PDNs, and RPDNs were evaluated using a mouse model infected with *Py*BY265 and a modified 4-day suppression test method. Briefly, ICR male mice were infected by administering an intraperitoneal 1.0×10^7 saline suspension of parasitized RBCs and randomly divided into 14 groups, with 6 mice in each group. The normal group received no treatment, and 13 groups were infected with *Py*By265. The infected groups were treated 2 h after infection via tail-vein injection with the following solutions: saline (control group). DHA solution at a dose of 8.8 μmol/kg, RBC-PLGA solution at a dose of 10 μmol/kg, PDNs and RPDNs dispersions at doses of 2.2, 4.4, 8.8, 17.6, and 35.2 μmol/kg. Doses of DHA, PDNs, and RPDNs were selected based on the principle of extrapolating doses from animals to humans. The same treatment was administered continuously at the same time point for 4 days. The infection ratios of *Plasmodium* parasites were determined using smear microscopy on days 5 and 11. The average infection ratios and inhibition ratios of the different groups were analyzed (Sarkar et al., 2016). The infection and inhibition ratios were calculated as follows:

$$Infection\ ratio = \frac{Number\ of\ iRBCs}{Number\ of\ counted\ RBCs} \times 100\%$$

The survival and weight curves of the PDNs and RPDNs groups were

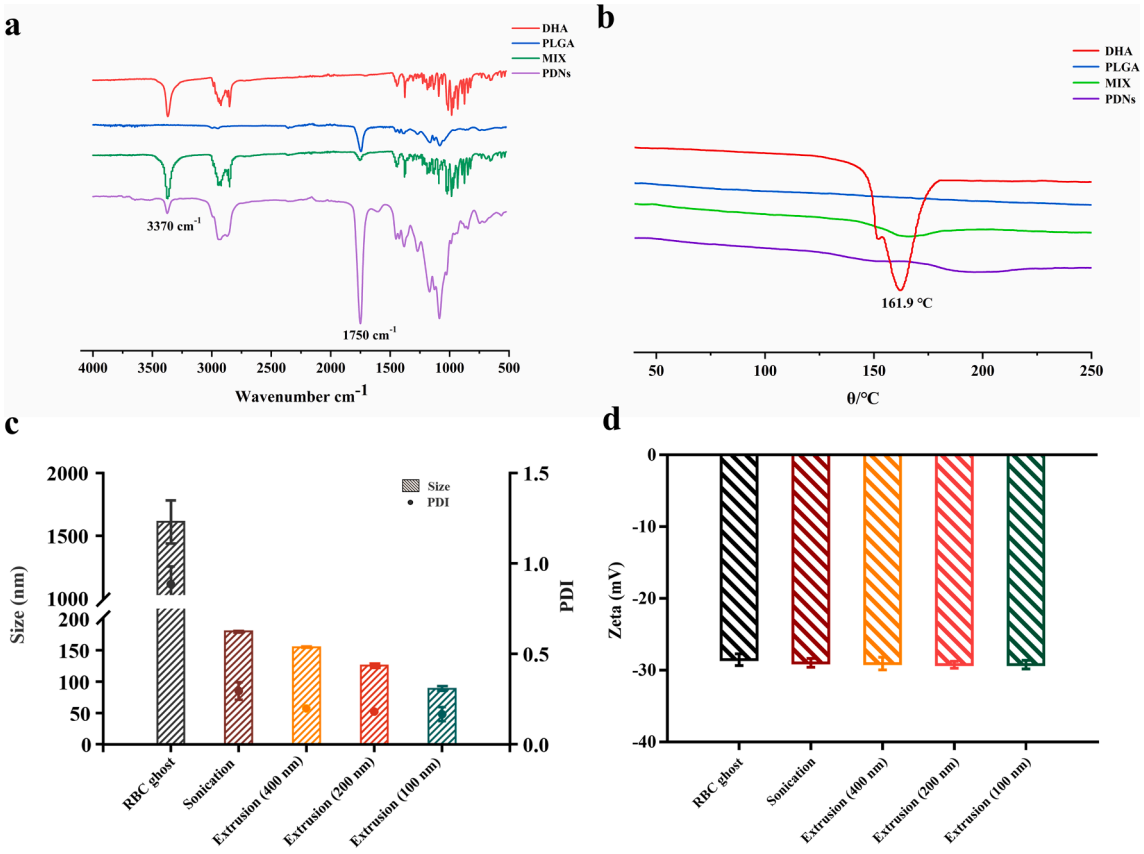

Fig. 1. (a) Infrared spectra of DHA, PLGA, MIX, and PDNs (b) DSC spectra of DHA, PLGA, MIX, and PDNs. The average particle size, PDI (c), and zeta potential (d) of RBC membranes and RVs after sonication and extrusion with 400-, 200-, 100-nm polycarbonate porous membranes. Data are presented as the mean ± SD (n = 3).

$$Inhibition\ ratio = \frac{Infection\ ratio\ of\ control\ group - Infection\ ratio\ of\ the\ treated\ group}{Infection\ ratio\ of\ control\ group - Infection\ ratio\ of\ normal\ group} \times 100\%$$

plotted. ED_{50}, ED_{90}, and median survival time (MST) were calculated using CompuSyn 1.0 and the Kaplan–Meier product-limit method. The mice were observed for 14 days.

2.14. Blood routine examination, liver function indexes, and histological analysis

After treatment for 7 or 14 days, blood and tissue samples were collected from the normal, control, DHA solution, and two high-dose PDNs and RPDNs groups. Whole-blood panel data (*i.e.*, WBC index: white blood cell, RBC index, HGB index: hemoglobin, HCT index: hematocrit, MCV index: mean corpuscular hemoglobin concentration, PLT index: platelets, RDW index: RBC distribution width) of normal, control, and two high-dose treatment groups were measured using a blood biochemical autoanalyzer (Mindray, China). Two important indicators of hepatic function, alanine aminotransferase (ALT) and aspartate aminotransferase (AST), were measured using commercial kits (Nanjing Jiancheng Biological Engineering Research Institute Co. Ltd., Nanjing, China). The heart, liver, spleen, lungs, and kidneys were collected and fixed with 4% paraformaldehyde solution. The samples were sectioned (4 μm thick) using conventional paraffin embedding, stained with hematoxylin and eosin (H&E), and examined under an optical microscope.

2.15. Statistical analysis

Data were analyzed using the GraphPad Prism software (version 6.0; GraphPad Software, Inc., San Diego, CA, USA) and are presented as the mean ± standard deviation. IBM SPSS Statistics (version 22.0; IBM Corp., Armonk, NY, USA) was used to analyze statistical differences. Statistical significance was set at $P \leq 0.05$.

3. Results and discussion

3.1. Preparation and formulation optimization of PDNs

The DHA concentration (X_1), the mass ratio of TPGS to PLGA (X_2), and stirring speed (X_3) were determined as independent variables, those markedly affecting the particle size (Y_1), zeta potential (Y_2), and EE (Y_3). The latter three factors were used as dependent variables. The regression equations were established via a three-factor BBD (Table S2):

$Y_1 = 74.89 + 7.05X_1 - 1.79X_2 + 0.20X_3 - 1.83X_1X_2 - 1.73X_1X_3 - 0.42X_2X_3 + 2.95{X_1}^2 + 2.85{X_2}^2 + 1.00{X_3}^2$

($R^2 = 0.9024$ $P_1 < 0.05$)

$Y_2 = -20.8 + 3.65X_1 - 0.17X_2 - 0.95X_3 + 0.75X_1X_2 - 1.50X_1X_3 + 1.20X_2X_3 - 0.06{X_1}^2 - 0.21{X_2}^2 + 1.24{X_3}^2$

($R^2 = 0.9555$ $P_2 < 0.05$)

$Y_3 = 41.04–13.81X_1 + 1.21X_2 + 5.3X_3 + 5.48X_1X_2 - 1.49X_1X_3 - 3.2X_2X_3 + 9.16{X_1}^2 + 12.7{X_2}^2 + 7.42{X_3}^2$

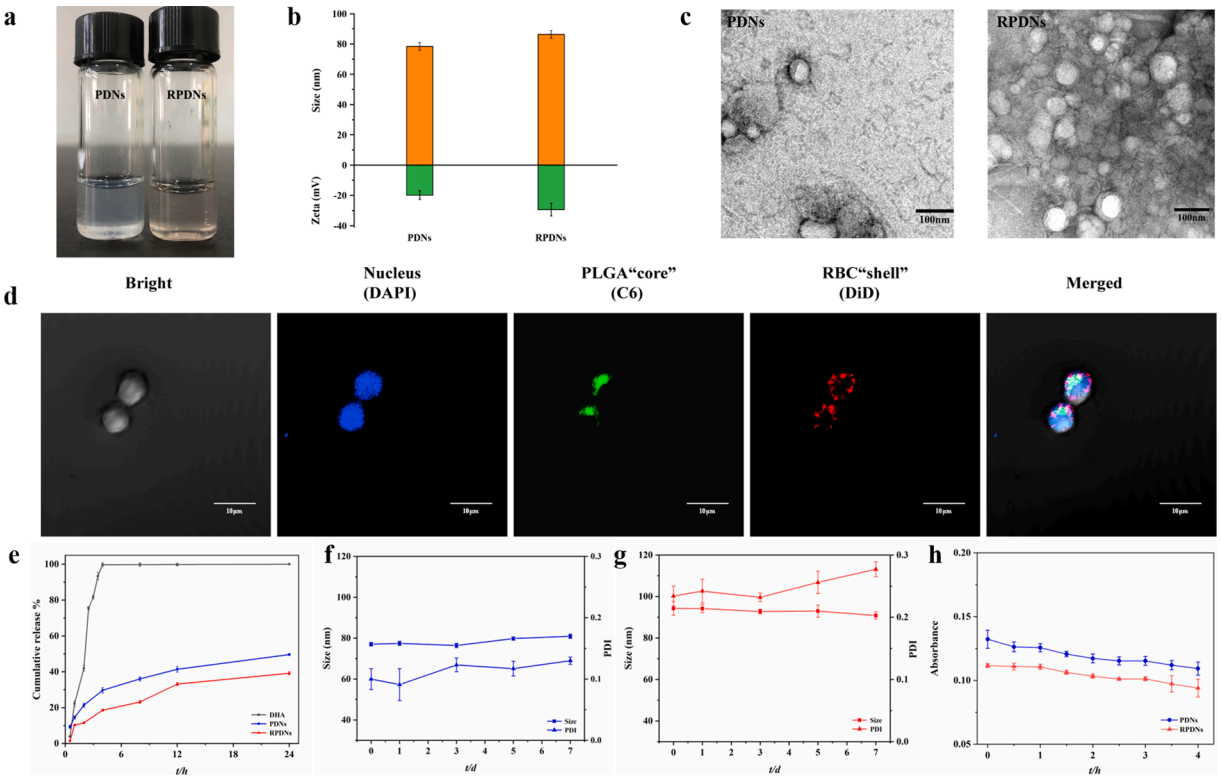

Fig. 2. (a) Morphology of PDNs and RPDNs. (b) Particle size and zeta potential of PDNs and RPDNs (mean ± SD, n = 3). (c) Transmission electron micrographs of PDNs and RPDNs (d) Confocal laser scanning micrographs of RPDNs internalization by cells, nucleus (blue), PLGA "core" (green), and RBC "shell" (red). (e) Cumulative release curves of DHA, PDNs, and RPDNs. (f) Particle size and PDI of PDNs after placement in water for 7 days. (g) Particle size and PDI of RPDNs after being placed in water for 7 days. (h) Serum stability of PDNs and RPDNs. Data are presented as mean ± SD (n = 3).

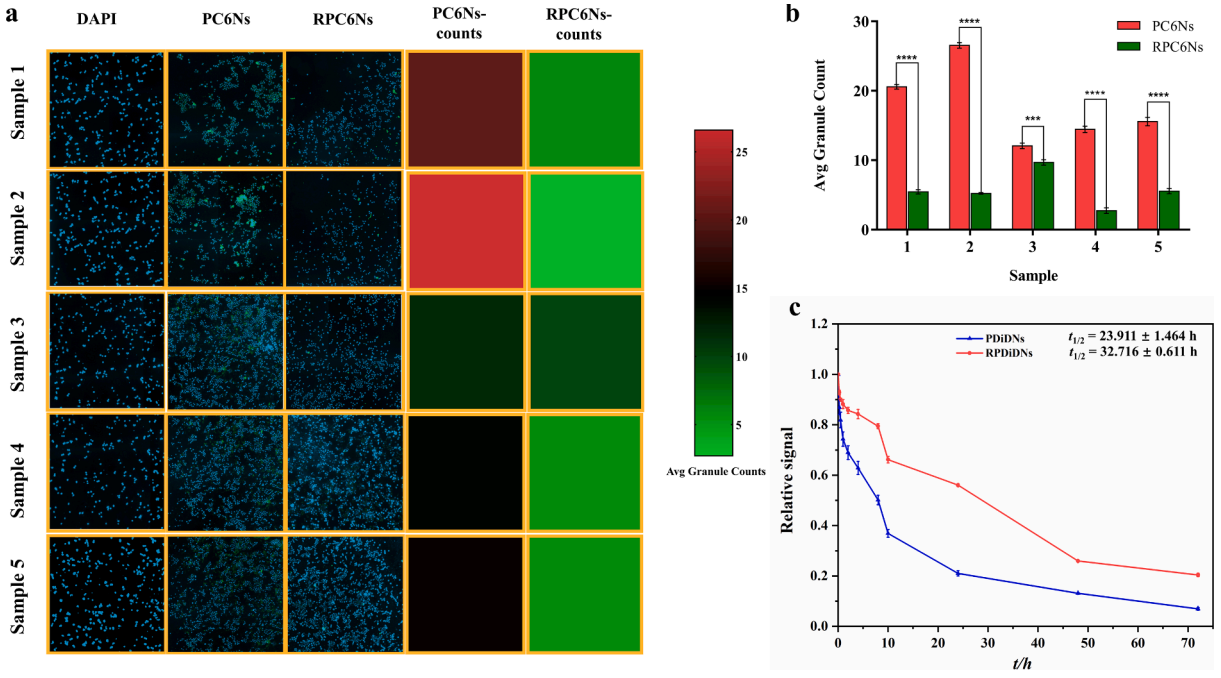

Fig. 3. (a) Images of PC6Ns and RPC6Ns phagocytosed by RAW 264.7 macrophages after 3 h of incubation, and heat map of the average granule counts of PC6Ns and RPC6Ns. (b) Average granule count of PC6Ns and RPC6Ns (****$P < 0.01$, ***$P < 0.05$, n = 5). (c) Blood circulation of PDiDNs and RPDiDNs in ICR mice. Data are presented as mean ± SD (n = 5).

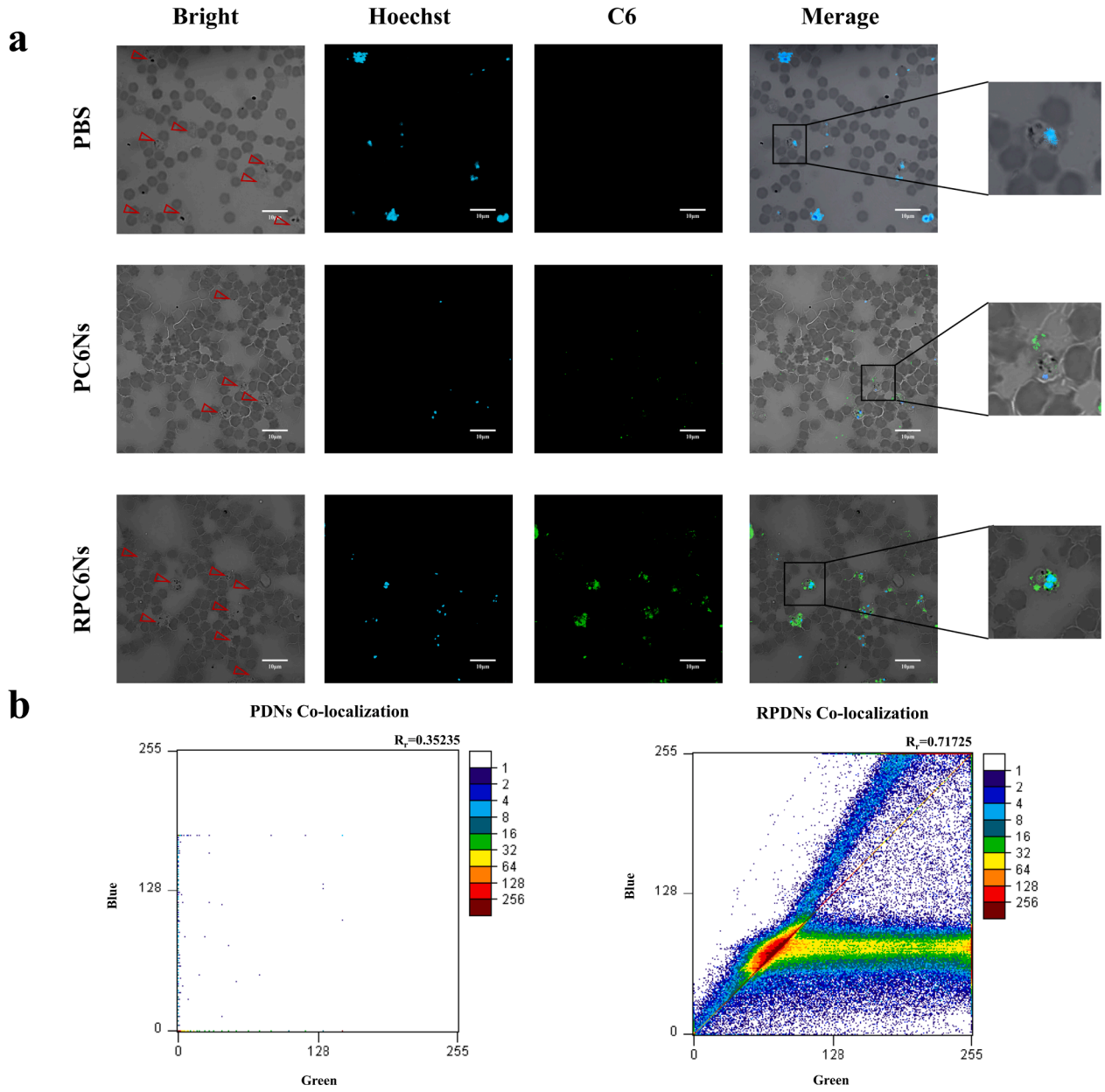

Fig. 4. (a) Confocal fluorescence microscopic analysis of the interaction of C6-labeled PDNs and RPDNs with iRBCs (the red triangles indicate iRBCs). (b) Colocalization scatter plots of PDNs and RPDNs.

($R^2 = 0.9698$ $P_3 < 0.05$)

According to the fitting equation and as shown in the three-dimensional effect map (Figure S1), the optimized formulation was obtained, that was, the concentration of DHA in PDNs was 1.0 mg/mL, the mass ratio of TPGS to PLGA was 10.28%, and stirring speed was 867 r/min, respectively. The absolute deviation between experimental and predicted values of the model (Table S3) was < 10%, indicating that the optimized model could accurately predict the nanoparticle size, zeta potential and EE.

3.2. Characterization of PDNs using FT-IR and DSC

The FT-IR spectra of DHA, PLGA, MIX, and PDNs lyophilized powder are shown in Fig. 1a. The strong absorbance of band appearing at 1750 cm^{-1} is related to the carbonyl group vibration of PLGA. DHA exhibited a characteristic absorption peak of the –OH group at 3370 cm^{-1}. The FT-IR spectrum of MIX was a physical overlay of the spectra of its two ingredients, while the characteristic absorption peak of DHA in PDNs was notably weakened. This implies that DHA was embedded in the nanoparticle core. To examine the physical state of DHA in PDNs, DSC curves of DHA, PLGA, MIX, and PDNs were shown Fig. 1b. The endothermic melting peak of DHA appeared at approximately 161.9 ° C. Conversely, no DHA melting peak observed for the PDNs. These findings suggest that DHA in the PDNs essentially existed in an amorphous or solid-solution state.

3.3. Preparation and characterization of RVs

RVs were prepared using sonication and extrusion methods. The average diameter of the RBC ghost was 2–3 μm (Fig. 1c). After sonication and extrusion through 400-, 200-, and 100-nm polycarbonate films, the product diameter decreased successively, eventually resulting in a clear colored RVs dispersions with an average vesicle size of 85.6 ± 2.39 nm and a narrow PDI ranging 0.152 ± 0.017. Inverted microscopy and TEM

Table 1
Infection and inhibition ratios of ICR mice.

Groups	Dose	Infection ratio on day 5	Inhibition ratio on day 5	Infection ratio on day 11
	(μmol/kg)	(%)	(%)	(%)
Control	saline	27.71 ± 1.56	–	–
RBC-PLGA	10	25.83 ± 1.22	–	–
DHA	8.8	11.40 ± 0.71	58.74 ± 3.78	42.86 ± 2.86
PDNs	2.2	7.37 ± 0.79	73.42 ± 2.18	29.02 ± 0.10
	4.4	6.06 ± 0.59	78.11 ± 2.26	22.82 ± 1.92
	8.8	4.66 ± 0.46	83.13 ± 2.12	18.89 ± 0.02
	17.6	3.51 ± 0.59	87.32 ± 1.99	13.93 ± 4.09
	35.2	2.49 ± 0.45	91.00 ± 1.73	5.19 ± 1.73
RPDNs	2.2	5.80 ± 0.43	78.95 ± 2.62*	11.87 ± 1.99
	4.4	4.46 ± 0.51	83.85 ± 2.24*	9.37 ± 0.33
	8.8	3.19 ± 0.61**	88.39 ± 2.69**	7.53 ± 1.01**
	17.6	2.17 ± 0.29	92.15 ± 1.05*	1.93 ± 0.92
	35.2	0.89 ± 0.41	96.78 ± 1.52*	0.83 ± 0.19

** $P < 0.05$: RPDNs *vs*. PDNs or DHA solution under the same dose.
* $P < 0.05$: RPDNs *vs* PDNs under the same dose.

analysis showed that the extruded RBC ghosts were spherical vesicles (Figure S2). Furthermore, zeta potentials of RVs of different treatments were examined (Fig. 1d); the average zeta potential of all RVs products were approximately −29 mV, not affected by the sonication or extrusion processes, which is consistent with the results of a previous report (Wang et al., 2019). The prepared RVs displayed good dispersion, which was beneficial for preparing biomimetic nanoparticles with uniform size distribution and reduced aggregation.

3.4. Preparation and characterization of PDNs and RPDNs

PDNs were generated with an optimized nano-platform via a nano-precipitation method. Furthermore, the PDNs were enveloped in extracted RVs using a co-extrusion method and assembled into RPDNs. The PDNs and RPDNs were translucent liquid preparations with a uniform appearance (Fig. 2a). The particle sizes of PDNs and RPDNs were examined using DLS. As shown in Fig. 2b, the diameters and PDI increased from 78.4 ± 2.19 nm and 0.112 ± 0.023 of PDNs to 86.4 ± 2.54 nm and 0.179 ± 0.011 of RPDNs, most likely due to the RBC membrane thickness of 7–8 nm (Hu et al., 2013). Based on surface zeta potential analysis, PDNs and RPDNs exhibited zeta potential of –19.7 ± 2.86 mV and −29.2 ± 4.19 mV, respectively. The presence of negatively charged sialic acid residues at the glycan terminus on the RBC membrane can exhibit a charge asymmetry on both sides, i.e., negatively charged on the outside of RBC membrane and positively charged on the inside of RBC membrane. The negative charge of PDNs and the positive charge within RVs can create an electrostatic interaction (Luk et al., 2014). The zeta potential of RPDNs was relatively close to that of the RVs. TEM analysis of PDNs and RPDNs revealed a uniform spherical morphology (Fig. 2c). In addition, RPDNs showed a core-shell nanostructure, with PDNs "core" and RBC "shell membrane," indicating that the RBC membrane was successfully cloaked on the surface of PDNs. To further verify the integrity of the core-shell nanoparticles, we performed fluorescence colocalization analysis. PLGA was loaded with C6 fluorophore to characterize RPDNs core, and the RBC membrane was labeled with DiD. Then, the dual-fluorescently labeled nanoparticles were incubated with RAW 264.7 cells. The resulting fluorescence image (Fig. 2d) revealed that most of the C6 fluorophore (green, representing PLGA "core") was co-located with DiD (red, representing RBC membrane "shell"), indicating complete "core-shell" structure of RPDNs.

3.5. Drug loading capacity, in vitro release assay, and preliminary stability study

EE and DL of the prepared nanoparticles were evaluated, and the average EE and DL were found to be 70.10 ± 0.79% and 1.21 ± 0.09%, respectively. The drug-release profile was examined to evaluate the sustained-release features of PDNs and RPDNs. Considering possible DHA degradation in PBS (Bai et al., 2021), we used 30% ethanol-PBS solution as the release media. As shown in Fig. 2e, the DHA exhibited a markedly rapid release rate, demonstrating almost complete release within 4 h. After 24 h of incubation, 39.23% and 48.28% of DHA was released from RPDNs and PDNs respectively. In addition, the cumulative amounts of DHA released from RPDNs at determined time points were correspondingly lower than those from PDNs. The enhanced sustained-release effect of RPDNs might be attributed to the RBC membrane physical barrier efficacy. To examine the effect of release media on the release pattern of nanoparticles, we investigated the release of nanoparticles loaded with artemisinin (ART) in PBS and 30% ethanol-PBS. We used ART as the model drug, which was relatively stable in PBS. As shown in Figure S3, the cumulative amounts of ART released from RBC membrane cloaked nanoparticles were lower than others groups in PBS and 30% ethanol-PBS solution. The 30% ethanol-PBS solution had less effect on the release pattern of nanoparticles. The size distribution and PDI were assessed to determine the preliminary stability of PDNs and RPDNs in water. The results demonstrated that the size distribution of PDNs (Fig. 2f) and RPDNs (Fig. 2g) in water remained relative uniform for 7 days (4 ° C), respectively. The PDIs of both PDNs and RPDNs were < 0.3, with satisfactory dispersion. In the serum stability tests, the previously absorbance method was used to monitor particle size changes in the presence of FBS (Fang et al., 2010). The larger particles induce higher light scatting, aggregation of unstable particles can be observed by monitoring the increase in the absorbance value (Guo et al., 2015; Hu et al., 2011). Both PDNs and RPDNs absorbance curves exhibited without significant change of absorbance values, indicating a satisfactory serum stability of PDNs and RPDNs (Fig. 2h).

3.6. In vitro hemolysis assay

Intravenous administration is the suitable route for nanoparticle delivery systems for malaria treatment. Therefore, the blood compatibility of RPDNs was further evaluated by performing a hemolysis experiment. After incubation with different concentrations of PDNs and RPDNs for 3 h, no marked hemolysis was observed in the whole blood samples. Furthermore, the absorbance of the supernatant of incubation samples were measured using an ultraviolet–visible spectrophotometer, and the hemolysis rate was calculated. The hemolysis rates for both PDNs and RPDNs, at different concentrations, were < 5% (Figure S4). These findings indicate that PDNs and RPDNs do not induce RBC hemolysis in 3 h.

3.7. Macrophage uptake study

The immune compatibility of nanoparticles can seriously impact their circulation time *in vivo* as well as clinical efficacy. Whether RPDNs possess the same immune compatibility as RBC was therefore investigated. RAW 264.7 cells (murine macrophage) were used to examine the antiphagocytic ability of RPDNs *in vitro*. PLGA nanoparticles was labeled with C6 to probe the prepared nanoparticles. Subsequently, PC6Ns and RPC6Ns were incubated with RAW 264.7 cells for 3 h in five identical microplate wells. The green fluorescence intensity of the RPC6Ns groups was weaker than that of the PC6Ns groups (Fig. 3a). Following the uptake of C6-labeled nanoparticles by RAW 264.7 cells, C6 was found mainly distributed in the cell membrane and plasma. The weak fluorescence intensity of RPC6Ns group indicated their poor uptake by macrophages. Furthermore, in the Endocytosis Module of the ImageXpress Pico Automated Cell imaging system, dual fluorescence channel

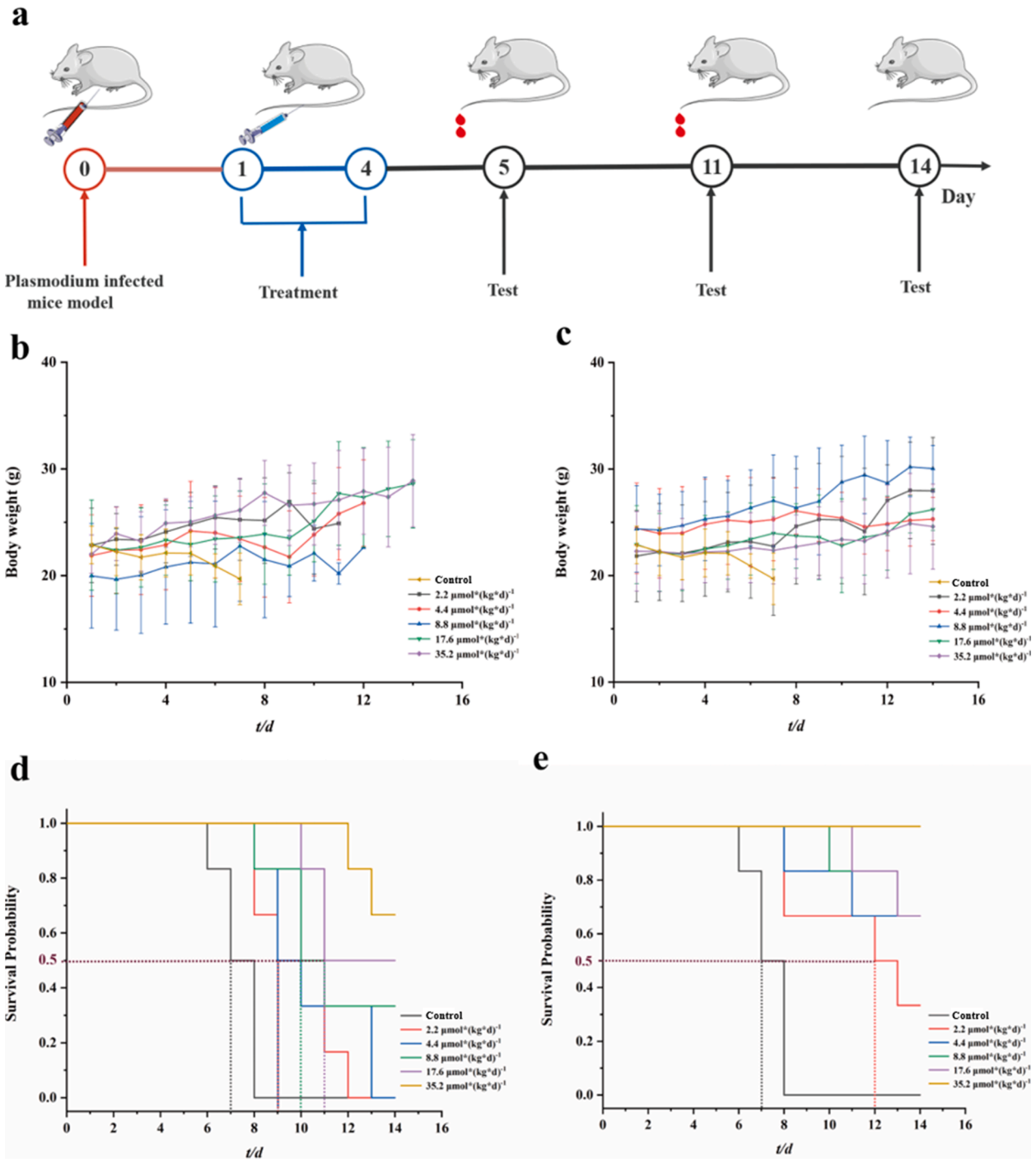

Fig. 5. (a) Establishment of a *Plasmodium*-infected model and treatment plan. Weight of mice receiving (b) PDNs treatment and control and (c) RPDNs treatment and control. Survival curve of mice receiving (d) PDNs treatment and control and (e) RPDNs treatment and control.

Table 2
ED_{50} and ED_{90} of mice groups treated with PDNs and RPDNs.

Concentration (μmol/kg)	PDNs	RPDNs
ED_{50}	0.53 ± 0.01	0.13 ± 0.05*
ED_{90}	14.48 ± 0.23	8.13 ± 0.18#

* $P < 0.05$: the ED_{50} of RPDNs *vs* PDNs under the same dose.
\# $P < 0.05$: the ED_{90} of RPDNs *vs* PDNs under the same dose.

analysis (green and blue) showed that the average granule counts of the PC6Ns groups were higher than those of the RPC6Ns groups (Fig. 3a). The average granule counts were related to the number of C6-labeled nanoparticles (green) attached to RAW 264.7 cells (blue). The average granule counts of RPC6Ns groups were significantly lower than those of PC6Ns groups ($P < 0.05$, Fig. 3b). Furthermore, quantitative analysis of cellular uptake using flow cytometry revealed that the uptake by RAW 264.7 cells of RPC6Ns was significantly lower than that of PC6Ns ($P < 0.05$, Figure S5). Collectively, these findings indicate that RBC membranes coated nanoparticles effectively prevented macrophage-mediated phagocytosis. RBCs are the most abundant cells in the blood,

Table 3
Routine blood parameters of ICR normal mice and treatment mice.

	Unite	Normal-mice	Control-*Py*BY265 infected mice	PDNs-*Py*BY265 infected mice	RPDNs-*Py*BY265 infected mice
WBC	10^9/L	4.40 ± 0.24	199.10 ± 2.12	9.00 ± 0.56	7.97 ± 0.47
RBC	10^{12}/L	9.55 ± 0.37	2.16 ± 0.23	8.45 ± 0.34	7.55 ± 0.27
HGB	g/L	138.67 ± 4.19	62.13 ± 1.27	139.33 ± 6.51	136.33 ± 8.50
HCT	CV%	42.27 ± 2.46	16.52 ± 0.21	44.37 ± 0.91	43.13 ± 1.96
MCV	fL	49.97 ± 0.21	76.71 ± 1.22	51.20 ± 3.31	52.67 ± 3.37
MCH	Pg	16.90 ± 0.29	18.73 ± 0.34	16.20 ± 0.95	16.57 ± 0.81
MCHC	g/L	315.33 ± 4.92	375.21 ± 5.23	317.67 ± 2.52	316.01 ± 7.10
PLT	10^9/L	588.33 ± 51.42	398.12 ± 13.29	476.33 ± 71.19	487.33 ± 14.84
RDW	CV%	15.67 ± 0.54	19.20 ± 1.32	15.87 ± 2.47	17.03 ± 1.37

with approximately 5 million cells/μL. The critical factor determining the long-term survival of RBCs is their surface make-up, composed of intricate "self-marker" membrane proteins that actively bypass immune surveillance. Our data suggested that RBC membrane-coated nanoparticles exhibited some immune-evasive properties.

3.8. In vivo blood circulation study

The RBC membrane-coated nanoparticles are superior to unmodified nanoparticles for bypassing macrophage-mediated systemic clearance, resulting in a prolonged blood circulation time (Gao et al., 2017; Zhou et al., 2016). Therefore, PLGA nanoparticles was labeled with DiD to probe the prepared nanoparticles, ICR mice (male, 6–8 weeks old) were used as a model to investigate the *in vivo* blood circulation of the prepared nanoparticles. The RPDiDNs displayed a greater blood retention time and longer elimination half-life than PDiDNs (Fig. 3c). After injection for 24 and 48 h, 56% and 26% of fluorescence intensity in RPDiDNs groups were detected, respectively. However, those were reduced to 21% and 13% in PDiDNs groups. The elimination half-life ($t_{1/2}$) of the RPDiDNs was 32.716 ± 0.611 h, which is longer than that of PDiDNs (23.911 ± 1.464 h). The mean residence time of RPDiDNs (47.029 ± 1.041 h) was significantly higher than that of PDiDNs (35.959 ± 2.573 h) ($P < 0.05$). The extended blood circulation time of the RBC-membrane-coated nanoparticles could be explained by their immune compatibility. The long-term circulatory effect of RBC membrane-cloaked nanoparticles is mediated by a series of membrane proteins present on the membrane surface. CD47, a representative marker and an immunomodulatory protein, previously evaluated in RBC membrane-cloaked nanoparticles (Brown, 2001; Oldenborg et al., 2000), plays a major role in the long-term circulation of nanoparticles following intravenous administration (Hu et al., 2013). In addition, RBC membrane-coated nanoparticles could overcome the rapid elimination of DHA to a certain extent.

3.9. Assessment of in vitro targeting ability of RPDNs

The adhesion of uninfected RBCs to infected RBC (rosetting) resulted in the parasites invasion to normal RBCs. The RBC membrane-encapsulated nanoparticles were expected to have targeting affinity and adhesion effect to iRBCs. To confirm the targeting effects of RPDNs, iRBCs labeled with Hoechst 33342 (blue) were incubated with C6-loaded PLGA nanoparticles (green). After incubation for 2 h, the fluorescence intensity of C6 in the cells was qualitatively detected using confocal laser scanning microscopy. An increasing fluorescence intensity of nanoparticles were found on the surface of iRBCs in the RPC6Ns group, compared to that in the PC6Ns group (Fig. 4a). Colocalization image analysis was utilized to further identify the targeting potence of RPDNs. The iRBCs are represented by the blue channel in the scatter plot, while nanoparticles are represented by the green channel (Fig. 4b). The RPC6Ns group demonstrated a linear relationship between green and blue channels, while no linear correlation was noted in the PC6Ns group. The Pearson correlation coefficient of the RPC6Ns group was 0.7173, indicating a correlation between the distribution of RPDNs and iRBCs.

3.10. In vivo antimalarial activity of RPDNs

The *in vivo* antimalarial activities of PDNs and RPDNs dispersions, and DHA solution were examined using a 4-day suppression test and further compared using the infection and inhibition ratios on day 5, the infection ratio on day 11, ED_{50}, ED_{90}, changes in body weight, and survival curves.

The inhibition ratio of both PDNs and RPDNs groups was > 70% at all examined doses, increasing in a dose-dependent manner (Table 1 and Fig. 5). At the middle dose (8.8 μmol/kg), the inhibition ratio of RPDNs (88.39 ± 2.69%) was markedly superior to that of PDNs (83.13 ± 2.12%) or DHA solution (58.74 ± 3.78%) ($P < 0.05$, n = 6) on day 5. In addition, the inhibition ratios of RPDNs were significantly higher than those of PDNs at all five doses on day 5 ($P < 0.05$). Compared with the control group, the PDNs (Fig. 5b) and RPDNs groups (Fig. 5c) did not exhibit significantly changes in body weights. Furthermore, the infection ratio of RPDNs groups on day 11 was lower than that of the PDNs groups at the same dose. Therefore, the antimalarial effect of the RPDNs was notably improved compared with that of PDNs and DHA solutions.

The ED_{50} and ED_{90} values of RPDNs (0.13 ± 0.05 μmol/kg and 8.13 ± 0.18 μmol/kg respectively) were significantly lower than those of PDNs (0.53 ± 0.01 μmol/kg and 14.48 ± 0.23 μmol/kg respectively) and DHA solution (0.87 ± 0.27 μmol/kg and 17.67 ± 3.38 μmol/kg respectively) ($P < 0.05$, n = 6) (Table 2). The ED_{50} and ED_{90} values of the DHA solution were gained from our previous study (Wang et al., 2021), which were conducted under the same controlled conditions. All mice in the high-dose RPDNs groups survived for 14 days (Fig. 5e), in which was superior to all other treatment groups. The MST of the RPDNs groups at each dose was correspondingly longer than those of PDNs groups. Overall, based on the observed infection ratio, inhibition ratio, ED_{50}, ED_{90}, and MST, it can be inferred that RPDNs enhanced antimalarial efficacy compared to PDNs. This phenomenon might be explained as follows: (i) RPDNs with RBC membrane, acting as diffusion barriers, could achieve sustain drug release for relatively longer time periods compared with PDNs. (ii) RPDNs coated with RBC membranes could evade phagocytosis by macrophages and systemic clearance, which prolonged the blood circulation time and the action time of DHA in the body. (iii) RPDNs benefited from membrane proteins of RBCs and could target the iRBCs and increase DHA concentration in parasites.

3.11. In vivo safety study

The safety of the nanoparticles is as important as their effectiveness. Thus, to assess their biosafety, possible adverse effects of RPDNs were examined after 14 days of treatment. The RBCs, WBCs, HCT, and HGB indexes of treated ICR mice were all within the reference range even at high-dose for both PDNs and RPDNs groups (Table 3). However, abnormal blood indexes were observed in the control group (high WBC index; high MCV index; low RBC count, HGB, HCT, and PLT indexes), which could be attributed to liver damage and anemia in *Py*By265-infected mice. Routine blood tests for normal ICR mice were preformed after 14 days of DHA, high-dose PDNs (35.2 μmol/kg), and RPDNs (35.2 μmol/kg) treatment (Figure S6). RBC, WBC, HCT, MCV, HGB, and PLT indexes did not vary among treated mice. The normal values of liver function indexes (ALT and AST) suggested that the prepared

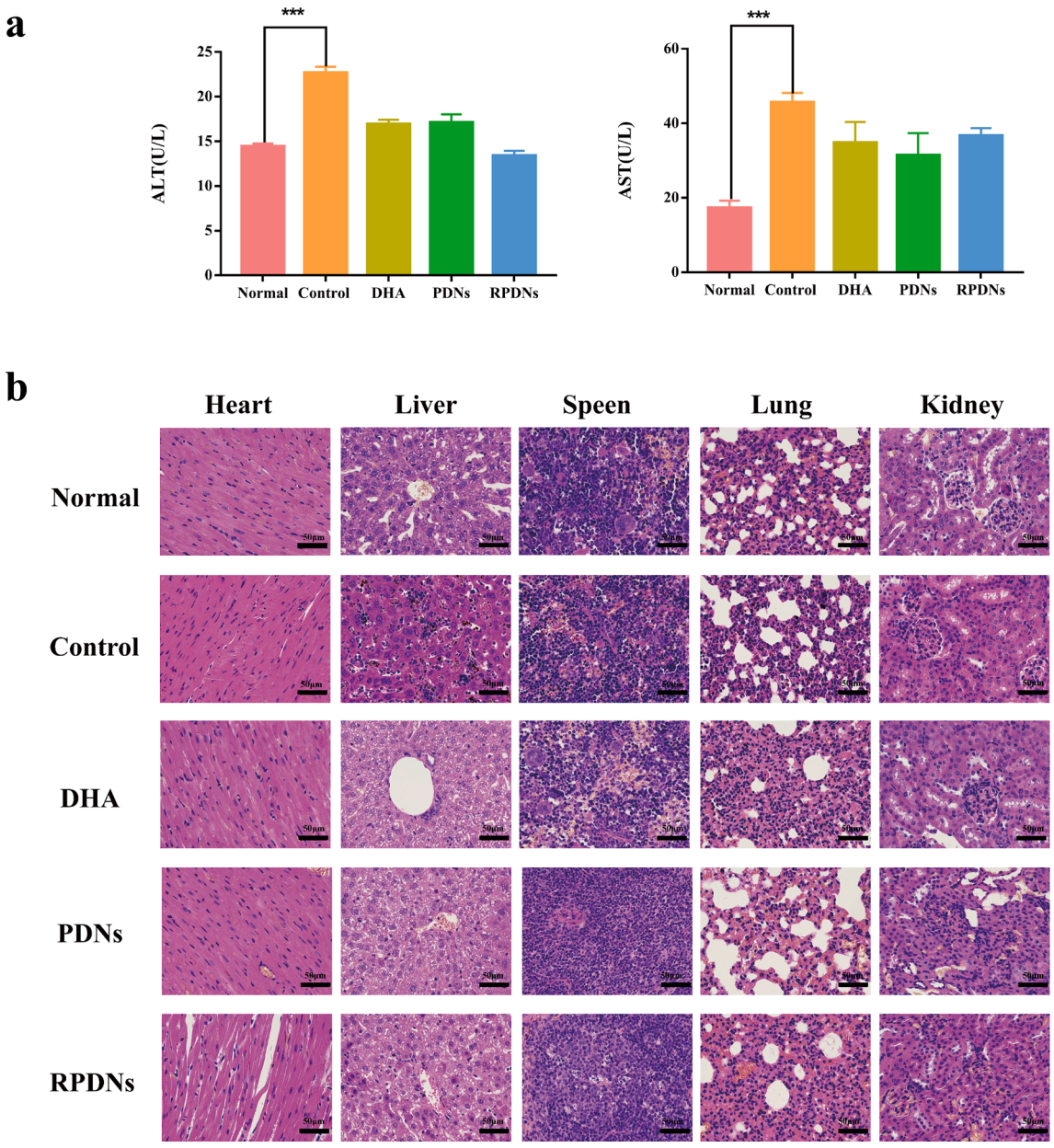

Fig. 6. (a) Biochemical assays of hepatic functions. ALT, alanine aminotransferase; AST, aspartate aminotransferase(***$P < 0.05$, n = 5), (b) H&E-stained images of main organs from ICR mice after following various treatments.

nanoparticles did not induce notable hepatic toxicity (Fig. 6a). Marked differences were observed between the control and normal groups. H&E staining revealed no substantial change in the main organs (including heart, liver, spleen, lung, and kidneys) of the treated groups, instead of control group (Fig. 6b). Histopathological abnormalities were detected in H&E-stained tissue sections of the control group. Malarial pigments were largely deposited in liver tissue sections. The structure of the liver plate was damaged, and hepatic sinusoids showed a large number of infiltrated inflammatory cells. The white pulp was considerably reduced in the pathological section of the spleen, while the red pulp was filled with malarial pigment. The lung tissue section displayed granulocytopenia and a small amount of brown pigment deposited in the alveolar walls. However, histopathological stains were normal in the examined organs of other treatment groups. Overall, these findings confirmed the good biocompatibility of RPDNs, which could be a promising and safe candidate for antimalaria therapy.

4. Conclusion

We developed erythrocyte-encapsulated biomimetic PLGA nanoparticles (RPDNs), which were loaded with DHA as the core and the RBC membrane as a cloak, to afford a more potent treatment strategy against malaria. The resulting RPDNs showed suitable pharmaceutical properties, including a high encapsulation rate, sustained drug release, satisfactory anti-phagocytosis effect *in vitro*, and iRBCs targeting ability. Moreover, RPDNs with a low dosage of ED_{90} exhibited improved antimalarial activity compared with PDNs. Furthermore, RPDNs displayed a desirable safety profile without significant side effects.

The present study explores the therapeutic advantages of RPDNs for treating malaria. The prepared RBC membrane cloaked DHA nanoparticles is a potential candidate for the management of malaria.

CRediT authorship contribution statement

Hengtong Zuo: Investigation, Methodology, Data curation, Formal analysis, Writing – original draft, Writing – review & editing. **Jihong Qiang:** Investigation, Methodology, Data curation, Formal analysis. **Yidan Wang:** Methodology, Validation. **Rongrong Wang:** Methodology, Validation, Visualization. **Geng Wang:** Methodology, Validation. **Liqing Chai:** Methodology, Validation. **Guolian Ren:** Funding acquisition, Supervision. **Yongdan Zhao:** Funding acquisition, Supervision, Validation. **Guoshun Zhang:** Methodology, Validation, Supervision, Writing – review & editing. **Shuqiu Zhang:** Project administration, Conceptualization, Resources, Validation, Funding acquisition, Writing – review & editing.

Declaration of Competing Interest

The authors declare that they have no known competing financial interests or personal relationships that could have appeared to influence the work reported in this paper.

Acknowledgements

This work was supported by the National Natural Science Foundation of China (Grant No.82173767 & Grant No.81803470); The Science and Technology Innovation Project of Institutions, Shanxi Province (2017148)

Appendix A. Supplementary material

Supplementary data to this article can be found online at https://doi.org/10.1016/j.ijpharm.2022.121665.

References

Aditya, N.P., Vathsala, P.G., Vieira, V., Murthy, R.S.R., Souto, E.B., 2013. Advances in nanomedicines for malaria treatment. Adv. Colloid Interface Sci. 201, 1–17. https://doi.org/10.1016/j.cis.2013.10.014.

Alanazi, F.K., Harisa, G.-D., Maqboul, A., Abdel-Hamid, M., Neau, S.H., Alsarra, I.A., 2011. Biochemically altered human erythrocytes as a carrier for targeted delivery of active ingredient: an in vitro study. Arch. Pharm. Res. 34 (4), 563–571. https://doi.org/ 10.1007/s12272-011-0406-7.

Ashley, E.A., Pyae Phyo, A., Woodrow, C.J., 2018. Malaria. Lancet 391 (10130), 1608–1621. https://doi.org/10.1016/s0140-6736(18)30324-6.

Bai, G., Gao, Y., Liu, S., Shui, S., Liu, G., 2021. pH-dependent rearrangement determines the iron-activation and antitumor activity of artemisinins. Free Radic. Biol. Med. 163, 234–242. https://doi.org/10.1016/j.freeradbiomed.2020.12.024.

Barabadi, H., Alizadeh, Z., Rahimi, M.T., Barac, A., Maraolo, A.E., Robertson, L.J., Masjedi, A., Shahrivar, F., Ahmadpour, E., 2019. Nanobiotechnology as an emerging approach to combat malaria: a systematic review. Nanomed.-Nanotechnol. Biol. Med. 18, 221–233. https://doi.org/10.1016/j.nano.2019.02.017.

Berry-Moorcrof, C., 2020. World Malaria Report 2020. World Health Organization, Switzerland, p. 2020.

Brown, E., 2001. Integrin-associated protein (CD47): an unusual activator of G protein signaling. J. Clin. Invest. 107 (12), 1499–1500. https://doi.org/10.1172/jci13315.

Cooke, B.M., Mohandas, N., Coppel, R.L., 2004. Malaria and the red blood cell membrane. Semin. Hematol. 41 (2), 173–188. https://doi.org/10.1053/j.seminhematol.2004.01.004.

Ding, D., Zhu, Q., 2018. Recent advances of PLGA micro/nanoparticles for the delivery of biomacromolecular therapeutics. Mater. Sci. Eng. C Mater. Biol. Appl. 92, 1041–1060. https://doi.org/10.1016/j.msec.2017.12.036.

Dong, X., Zhang, X., Wang, M., Gu, L., Li, J., Gong, M., 2021. Active ingredient-decorated nanostructured lipid carriers of active ingredient-protoporphyrin IX-transferrin combination for therapy of malaria. Int J Pharm. 605, 120813. https://doi.org/10.1016/j.ijpharm.2021.120813.

Edlund, P.O., Westerlund, D., Carlqvist, J., Wu, B.L., Jin, Y.H., 1984. Determination of artesunate and dihydroartemisinine in plasma by liquid chromatography with post-column derivatization and UV-detection. Acta Pharm Suec. 21, 223–234.

Efferth, T., 2017. From ancient herb to modern drug: Artemisia annua and artemisinin for cancer therapy. Semin. Cancer Biol. 46, 65–83. https://doi.org/10.1016/j.semcancer.2017.02.009.

Fang, R.H., Aryal, S., Hu, C.-M., Zhang, L., 2010. Quick synthesis of lipid-polymer hybrid nanoparticles with low polydispersity using a single-step sonication method. Langmuir. 26 (22), 16958–16962. https://doi.org/10.1021/la103576a.

Fang, R.H., Kroll, A.V., Gao, W., Zhang, L., 2018. Cell membrane coating nanotechnology. Adv. Mater. 30 (23), 1706759. https://doi.org/10.1002/adma.201706759.

Fröhlich, T., Hahn, F., Belmudes, L., Leidenberger, M., Friedrich, O., Kappes, B., Couté, Y., Marschall, M., Tsogoeva, S.B., 2018. Synthesis of artemisinin-derived dimers, trimers and dendrimers: investigation of their antimalarial and antiviral activities including putative mechanisms of action. Chem.-Eur. J. 24 (32), 8103–8113. https://doi.org/10.1002/chem.201800729.

Gao, M., Liang, C., Song, X., Chen, Q., Jin, Q., Wang, C., Liu, Z., 2017. Erythrocyte-membrane-enveloped perfluorocarbon as nanoscale artificial red blood cells to relieve tumor hypoxia and enhance cancer radiotherapy. Adv. Mater. 29 (35), 1701429. https://doi.org/10.1002/adma.201701429.

Gordi, T., Nielsen, E., Yu, Z., Westerlund, D., Ashton, M., 2000. Direct analysis of artemisinin in plasma and saliva using coupled-column high-performance liquid chromatography with a restricted-access material pre-column. J. Chromatogr. B Biomed. Sci. Appl. 742 (1), 155–162.

Guo, Y., Wang, D., Song, Q., Wu, T., Zhuang, X., Bao, Y., Kong, M., Qi, Y., Tan, S., Zhang, Z., 2015. Erythrocyte membrane-enveloped polymeric nanoparticles as nanovaccine for induction of antitumor immunity against melanoma. ACS Nano 9 (7), 6918–6933. https://doi.org/10.1021/acsnano.5b01042.

Hu, C.M., Fang, R.H., Luk, B.T., Chen, K.N., Carpenter, C., Gao, W., Zhang, K., Zhang, L., 2013. 'Marker-of-self' functionalization of nanoscale particles through a top-down cellular membrane coating approach. Nanoscale 5, 2664–2668. https://doi.org/10.1039/c3nr00015j.

Hu, C.-M., Zhang, L.i., Aryal, S., Cheung, C., Fang, R.H., Zhang, L., 2011. Erythrocyte membrane-camouflaged polymeric nanoparticles as a biomimetic delivery platform. Proc. Natl. Acad. Sci. U S A. 108 (27), 10980–10985. https://doi.org/10.1073/pnas.1106634108.

Li, C.H., Wang, X., Li, R.J., Yang, X.L., Zhong, Z.R., Dai, Y., Fan, Q.Z., Lin, Y., Zhang, R.T., Liang, T.T., Ye, Y., Zhou, M.L., 2019. Resveratrol-loaded PLGA nanoparticles functionalized with red blood cell membranes as a biomimetic delivery system for prolonged circulation time. J. Drug Deliv. Sci. Technol. 54, 6. https://doi.org/10.1016/j.jddst.2019.101369.

Luk, B.T., Jack Hu, C.-M., Fang, R.H., Dehaini, D., Carpenter, C., Gao, W., Zhang, L., 2014. Interfacial interactions between natural RBC membranes and synthetic polymeric nanoparticles. Nanoscale 6 (5), 2730–2737.

Luk, B.T., Zhang, L., 2015. Cell membrane-camouflaged nanoparticles for drug delivery. J. Control. Release 220, 600–607. https://doi.org/10.1016/j.jconrel.2015.07.019.

Melendez, V., Peggins, J.O., Brewer, T.G., Theoharides, A.D., 1991. Determination of the antimalarial arteether and its deethylated metabolite dihydroartemisinin in plasma by high-performance liquid chromatography with reductive electrochemical detection. J Pharm Sci. 80 (2), 132–138. https://doi.org/10.1002/jps.2600800209.

Mir, M., Ahmed, N., Rehman, A.U., 2017. Recent applications of PLGA based nanostructures in drug delivery. Colloids Surf. B Biointerfaces 159, 217–231. https://doi.org/10.1016/j.colsurfb.2017.07.038.

Mohandas, N., An, X., 2012. Malaria and human red blood cells. Med. Microbiol. Immunol. 201 (4), 593–598. https://doi.org/10.1007/s00430-012-0272-z.

Moxon, C.A., Grau, G.E., Craig, A.G., 2011. Malaria: modification of the red blood cell and consequences in the human host. Br. J. Haematol. 154 (6), 670–679. https://doi.org/10.1111/j.1365-2141.2011.08755.x.

Ndam, N.T., Moussiliou, A., Lavstsen, T., Kamaliddin, C., Jensen, A.T.R., Mama, A., Tahar, R., Wang, C.W., Jespersen, J.S., Alao, J.M., Gamain, B., Theander, T.G., Deloron, P., 2017. Parasites causing cerebral falciparum malaria bind multiple endothelial receptors and express EPCR and ICAM-1-binding PfEMP1. J. Infect. Dis. 215, 1918–1925. https://doi.org/10.1093/infdis/jix230.

Oldenborg, P.-A., Zheleznyak, A., Fang, Y.-F., Lagenaur, C.F., Gresham, H.D., Lindberg, F.P., 2000. Role of CD47 as a marker of self on red blood cells. Science 288 (5473), 2051–2054.

Ren, G., Chen, P., Tang, J., Guo, W., Wang, R., Li, N., Li, Y., Zhang, G., Wang, R., Zhang, S., 2020. In vivo and in vitro evaluation of dihydroartemisinin prodrug nanocomplexes as a nano-drug delivery system: characterization, pharmacokinetics and pharmacodynamics. Rsc Adv. 10 (29), 17270–17279.

Rowe, J.A., Claessens, A., Corrigan, R.A., Arman, M., 2009. Adhesion of Plasmodium falciparum-infected erythrocytes to human cells: molecular mechanisms and therapeutic implications. Expert. Rev. Mol. Med. 11, e16. https://doi.org/10.1017/s1462399409001082.

Santos-Magalhães, N.S., Mosqueira, V.C.F., 2010. Nanotechnology applied to the treatment of malaria. Adv. Drug Deliv. Rev. 62 (4-5), 560–575. https://doi.org/10.1016/j.addr.2009.11.024.

Sarkar, S., Siddiqui, A.A., Saha, S.J., De, R., Mazumder, S., Banerjee, C., Iqbal, M.S., Nag, S., Adhikari, S., Bandyopadhyay, U., 2016. Antimalarial activity of small-molecule benzothiazole hydrazones. Antimicrob. Agents Chemother. 60 (7), 4217–4228.

Smith, J.D., Rowe, J.A., Higgins, M.K., Lavstsen, T., 2013. Malaria's deadly grip: cytoadhesion of Plasmodium falciparum-infected erythrocytes. Cell Microbiol. 15 (12), 1976–1983. https://doi.org/10.1111/cmi.12183.

Spanjers, J.M., Städler, B., 2020. Cell membrane coated particles. Adv Biosyst. 4 (11), 2000174. https://doi.org/10.1002/adbi.202000174.

Wahlgren, M., Goel, S., Akhouri, R.R., 2017. Variant surface antigens of Plasmodium falciparum and their roles in severe malaria. Nat. Rev. Microbiol. 15 (8), 479–491. https://doi.org/10.1038/nrmicro.2017.47.

Walvekar, P., Gannimani, R., Govender, T., 2019. Combination drug therapy via nanocarriers against infectious diseases. Eur. J. Pharm. Sci. 127, 121–141. https://doi.org/10.1016/j.ejps.2018.10.017.

Wang, R., Ren, G., Chai, L., Guo, W., Li, Y., Wang, R., Zhao, Y., Zhang, S., 2021. Pharmacokinetics and antimalarial activities of reduction-responsive releasing dihydroartemisinin prodrug self-assembled nanoparticles in rodents. J. Drug Deliv. Sci. Technol. 63, 102515. https://doi.org/10.1016/j.jddst.2021.102515.

Wang, Y.i., Zhang, K., Qin, X., Li, T., Qiu, J., Yin, T., Huang, J., McGinty, S., Pontrelli, G., Ren, J., Wang, Q., Wu, W., Wang, G., 2019. Biomimetic nanotherapies: red blood cell based core-shell structured nanocomplexes for atherosclerosis management. Adv. Sci. (Weinh). 6 (12), 1900172. https://doi.org/10.1002/advs.201900172.

Wei, W., Cheng, W., Dai, W., Lu, F., Cheng, Y., Jiang, T., Ren, Z., Xie, Y., Xu, J., Zhao, Q., Yu, X., Yin, Y.i., Li, J., Dong, H., 2022. A Nanodrug coated with membrane from brain microvascular endothelial cells protects against experimental cerebral malaria. Nano Lett. 22 (1), 211–219. https://doi.org/10.1021/acs.nanolett.1c03514.

Xia, Q., Zhang, Y., Li, Z., Hou, X., Feng, N., 2019. Red blood cell membrane-camouflaged nanoparticles: a novel drug delivery system for antitumor application. Acta Pharm. Sin. B 9 (4), 675–689.

Xu, C.H., Ye, P.J., Zhou, Y.C., He, D.X., Wei, H., Yu, C.Y., 2020. Cell membrane-camouflaged nanoparticles as drug carriers for cancer therapy. Acta Biomater. 105, 1–14. https://doi.org/10.1016/j.actbio.2020.01.036.

Yam, X.Y., Niang, M., Madnani, K.G., Preiser, P.R., 2017. Three is a crowd - new insights into rosetting in Plasmodium falciparum. Trends Parasitol. 33 (4), 309–320. https://doi.org/10.1016/j.pt.2016.12.012.

Zhang, G., Dai, H., Ren, G., Xiao, X., Zhao, L., Wang, R., Zhang, S., 2018. Antimalarial activity and metabolism of dihydroartemisinin-derived dimer. Parasitol. Res. 117 (7), 2243–2254. https://doi.org/10.1007/s00436-018-5911-x.

Zhang, Y., Zhang, J., Chen, W., Angsantikul, P., Spiekermann, K.A., Fang, R.H., Gao, W., Zhang, L., 2017. Erythrocyte membrane-coated nanogel for combinatorial antivirulence and responsive antimicrobial delivery against Staphylococcus aureus infection. J. Control. Release 263, 185–191. https://doi.org/10.1016/j.jconrel.2017.01.016.

Zhou, H., Fan, Z., Lemons, P.K., Cheng, H., 2016. A facile approach to functionalize cell membrane-coated nanoparticles. Theranostics 6 (7), 1012–1022. https://doi.org/10.7150/thno.15095.

Zhou, X., Zhang, H. Z., Zhou, H. Y., Wang, J. B., Xiao, X. H., Zhao, R. H., Bai, Z. F., 2017. Methodological research for the promoting effect of Dendrobium moniliforme on macrophage phagocytosis based on high-content screeening. Acta Pharmaceutica Sinica. 52(5), 737-744. http://html.rhhz.net/YXXB/html/20170510.htm.

Zhu, H., Chen, H., Zeng, X., Wang, Z., Zhang, X., Wu, Y., Gao, Y., Zhang, J., Liu, K., Liu, R., Cai, L., Mei, L., Feng, S.-S., 2014. Co-delivery of chemotherapeutic drugs with vitamin E TPGS by porous PLGA nanoparticles for enhanced chemotherapy against multi-drug resistance. Biomaterials 35 (7), 2391–2400. https://doi.org/10.1016/j.biomaterials.2013.11.086.